Available online at www.sciencedirect.com
ScienceDirect
Earth and Planetary Science Letters 250 (2006) 470–485
EPSL
www.elsevier.com/locate/epsl

Xenon isotope systematics, giant impacts, and mantle degassing on the early Earth

Robert O. Pepin [a,*], Don Porcelli [b]

[a] School of Physics and Astronomy, University of Minnesota, 116 Church Street S. E., Minneapolis MN 55455, USA
[b] Department of Earth Sciences, Oxford University, Parks Road, Oxford OX1 3PR, UK

Received 22 December 2005; received in revised form 10 August 2006; accepted 18 August 2006
Available online 27 September 2006
Editor: R.W. Carlson

Abstract

The relationships between the major terrestrial volatile reservoirs are explored by resolving the different components in the Xe isotope signatures displayed by Harding County and Caroline CO_2 well gases and mid-ocean ridge basalts (MORB). For the nonradiogenic isotopes, there is evidence for the presence of components enhanced in the light $^{124-128}Xe/^{130}Xe$ isotope ratios with respect to the terrestrial atmosphere. The observation of small but significant elevations of these ratios in the MORB and well gas reservoirs means that the nonradiogenic Xe in the atmosphere cannot be the primordial base composition in the mantle. The presence of solar-like components, for example U–Xe, solar wind Xe, or both, is required.

For radiogenic Xe generated by decay of short-lived ^{129}I and ^{244}Pu, the $^{129}Xe_{rad}/^{136}Xe_{244}$ ratios are indistinguishable in MORB and the present atmosphere, but differ by approximately an order of magnitude between the MORB and well gas sources. Correspondence of these ratios in MORB and the atmosphere within the relatively small uncertainties found here significantly constrains possible mantle degassing scenarios. The widely held view that substantial early degassing of $^{129}Xe_{rad}$ and $^{136}Xe_{244}$ from the MORB reservoir to the atmosphere occurred and then ended while ^{129}I was still alive is incompatible with equal ratios, and so is not a possible explanation for observed elevations of $^{129}Xe/^{130}Xe$ in MORB compared to the atmosphere. Detailed degassing chronologies constructed from the isotopic composition of MORB Xe are therefore questionable.

If the present estimate for the uranium/iodine ratio in the bulk silicate Earth (BSE) is taken to apply to all interior volatile reservoirs, the differing $^{129}Xe_{rad}/^{136}Xe_{244}$ ratios in MORB and the well gases point to two episodes of major mantle degassing, presumably driven by giant impacts, respectively ~20–50 Ma and ~95–100 Ma after solar system origin assuming current values for initial $^{129}I/^{127}I$ and $^{244}Pu/^{238}U$. The earlier time range, for degassing of the well gas source, spans Hf–W calculations for the timing of a moon-forming impact. The second, later impact further outgassed the upper mantle and MORB source. A single event that degassed both the MORB and gas well reservoirs at the time of the moon-forming collision would be compatible with their distinct $^{129}Xe_{rad}/^{136}Xe_{244}$ ratios only if the post-impact iodine abundance in the MORB reservoir was about an order of magnitude lower than current estimates. In either case, such late dates require large early losses of noble gases, so that initial inventories acquired throughout the Earth must have been substantially higher.

The much larger $^{129}Xe_{rad}/^{136}Xe_{244}$ ratio in the well gases compared to MORB requires that these two Xe components evolve from separate interior reservoirs that have been effectively isolated from each other for most of the age of the planet, but are now seen within the upper mantle. These reservoirs have maintained distinct Xe isotope signatures despite having similar Ne isotope compositions that reflect similar degassing histories. This suggests that the light noble gas and radiogenic Xe isotopes are decoupled, with separate long-term storage of the latter. However, without data on the extent of heterogeneities within the upper

* Corresponding author. Tel.: +1 612 624 0819; fax: +1 612 624 4578.
E-mail addresses: pepin001@tc.umn.edu (R.O. Pepin), Don.Porcelli@earth.ox.ac.uk (D. Porcelli).

0012-821X/$ - see front matter
doi:10.1016/j.epsl.2006.08.014

mantle, this conclusion cannot be easily reconciled with geophysical observations without significant re-evaluation of present noble gas models. Nevertheless the analytic evidence that two different values of $^{129}Xe_{rad}/^{136}Xe_{244}$ exist in the Earth appears firm. If the uranium/iodine ratio is approximately uniform throughout the BSE, it follows that degassing events from separate reservoirs at different times are recorded in the currently available terrestrial Xe data.

Keywords: xenon; radionuclide daughters; mantle; atmosphere; moon; giant impacts; degassing

1. Introduction

There is strong evidence from dynamical modeling that Earth was impacted by massive bodies in the Mercury–Mars size range during its accretion, and that the moon formed from debris ejected by one of these collisions [1–3]. Such impacts likely powered degassing of volatiles from the Earth's interior, and escape of atmospheric gases to space, and so were key events in shaping the present atmosphere. Clues to the timing and extent of early noble gas losses are recorded in the abundances of xenon isotopes produced by two extinct radionuclides, $^{129}Xe_{rad}$ from β decay of ^{129}I ($\tau_{1/2}$= 15.7 Ma) and $^{131-136}Xe_{244}$ from spontaneous fission of ^{244}Pu ($\tau_{1/2}$=80.0 Ma). Amounts of $^{129}Xe_{rad}$ on Earth are much smaller than the amounts of parent ^{129}I in Earth-forming materials 4567 Ma ago, pointing to substantial losses of Xe and other volatiles during planet formation. One challenge has been to assess the effects of these losses on the initial volatile inventories and present-day compositions in different terrestrial reservoirs. Another has been to determine the times when the reservoirs were depleted [4–9] and their relation to the timing of giant impacts on Earth estimated from other evidence, e.g. Hf–W isotope systematics [10–15].

Xenon data from Earth's volatile reservoirs are evaluated here as mixtures of components acquired during accretion and generated on and in the planet by fractionation and radioactive decay. Discussion is focused primarily on calculated ratios of radiogenic ^{129}Xe to plutogenic ^{136}Xe in the atmosphere and in mantle Xe reservoirs, and on what their similarities or differences imply for reservoir interrelations and their geophysical and geochemical environments. These ratios are also used to obtain Xe–Xe "closure age" approximations of when the reservoirs began to retain daughter Xe isotopes after episodes of major volatile loss. Closure age estimates are useful in relating the results of this work to calculations of the timing of differentiation events in the early Earth and to the literature on terrestrial noble gas distributions, much of which is directed toward derivation of degassing chronologies.

The following analyses of the data reveal evidence for the presence of a mantle Xe component that is isotopically related to Xe in the sun and meteorites. Further, the relative proportions of radiogenic ^{129}Xe to plutogenic ^{136}Xe are essentially identical in the upper mantle and atmosphere but differ greatly from another interior reservoir. These results identify new and potentially powerful constraints on the origins and affiliations of mantle and atmospheric noble gases.

2. Data evaluation methods

2.1. Resolving daughter Xe isotopes in the atmosphere

Obtaining Xe isotopic constraints on relationships between the various terrestrial reservoirs, as well as the extent and timing of volatile losses, has been hampered by difficulties in resolving daughter Xe isotopes from nonradiogenic Xe. Contributions from ^{129}I and ^{244}Pu must be separated from an underlying nonradiogenic base composition. However, there is no common solar system Xe component that can provide a suitable atmospheric base. The composition used here is U–Xe, a component derived from comparison of terrestrial and meteorite data [16]. Hydrodynamic escape to space, driven by energy deposited in a giant impact or by strong ultraviolet radiation from the young sun, dissipates and isotopically fractionates a primordial atmosphere containing U–Xe [9,16–18]. The result is a fractionated U–Xe residue called "Nonradiogenic Earth Atmosphere" or NEA-Xe, to which decay products were later added [16–18] and are now clearly resolvable.

2.2. Resolving mantle Xe components

For the mantle, degassing histories are deduced from Xe found in MORB, crustal CO_2 well gases that have trapped mantle volatiles, and ocean island basalts (OIB). Despite pervasive atmospheric (Air-Xe) contamination [19–22], $^{129}Xe_{rad}$ is readily discernible, most clearly in MORB and well gases. However, plutonium-derived Xe is obscured by the masking presence of abundant heavy isotope Xe generated by fission of long-lived uranium-

Table 1
Isotopic compositions of xenon components used in the modelling

Compositon	^{124}Xe	^{126}Xe	^{128}Xe	^{129}Xe	^{130}Xe	^{131}Xe	^{132}Xe	^{134}Xe	^{136}Xe
Air-Xe [16,9]	2.337(07)	2.180(11)	47.15(05)	649.6(06)	=100	521.3(06)	660.7(05)	256.3(04)	217.6(02)
U–Xe[16,9]	2.928(10)	2.534(13)	50.83(06)	628.6(06)	=100	499.6(06)	604.7(06)	212.6(04)	165.7(03)
SW-Xe [16,9]	2.928(10)	2.534(13)	50.83(06)	628.6(06)	=100	499.6(06)	604.7(06)	220.7(09)	179.7(06)
Xe-Q [41,9]	2.810(13)	2.506(12)	50.77(16)	643.6(17)	=100	505.6(11)	617.7(11)	233.5(08)	195.4(06)
NEA-Xe [17,9]	2.337(07)	2.180(11)	47.15(05)	605.3(29)	=100	518.7(07)	651.8(13)	247.0(13)	207.5(13)
Average MORB-1	2.390(25)	2.224(21)	47.52(11)	706(10)	=100	524.1(11)	672.0(26)	272.2(28)	235.2(33)
Average MORB-2	2.393(24)	2.212(28)	47.40(13)	704.9(33)	=100	523.8(26)	672.1(32)	271.4(15)	234.4(16)
Kunz et al. MORB [6]	2.361(27)	2.210(16)	47.31(13)	709.8(33)	=100	524.3(27)	673.1(35)	272.7(15)	236.5(15)
Caroline well [22]	2.381(10)	2.214(10)	47.46(05)	709.0(04)	=100	521.7(03)	669.3(04)	271.5(01)	236.1(01)
Harding Co. well [22]	2.366(14)	2.226(13)	47.47(07)	714.2(04)	=100	522.6(03)	673.9(06)	278.7(02)	244.5(02)
$^{238}U_{sf}$ [42]	=0	=0	=0	≅0	=0	8.47(29)	57.17(47)	82.47(58)	=100
$^{244}Pu_{sf}$ [43]	=0	=0	=0	≅0	=0	24.8(15)	89.3(13)	93.00(50)	=100

Uncertainties ($\pm 1\sigma$) in the last two digits of the listed relative isotopic abundances are indicated in parentheses.

238, and while it has been identified in recent high precision data for Xe in MORB [6] and in well gases [22], there has been considerable uncertainty in accurately quantifying it. This is due both to the apparent scatter in the analyses and to difficulties in determining the composition of the nonradiogenic Xe component. The identity of this "primordial Earth mantle" (PEM) Xe clearly affects the calculated amounts of daughter Xe. Suggestions for the PEM constituent include nebular gases adsorbed on [17] or dissolved into [23] the growing planet from a dense primordial atmosphere, solar gases implanted in proto-Earth materials at solar wind (SW) and higher energies [22,24–26], meteoritic "Q-gases" carried by accreted planetesimals [27], and NEA-Xe or Air-Xe [6,8,28,29]. A critical observation is that only NEA-Xe, as defined above, can serve as the nonradiogenic Xe composition for the atmosphere; the others have heavy Xe isotope abundances that are too high [16]. However there is evidence, discussed in the next section, that the primordial component trapped in the mantle cannot be NEA-Xe.

The radiogenic and fissiogenic components of mantle Xe are determined, using the method developed by [22], by assuming that well-gas and MORB Xe are multicomponent mixtures of five independent components: PEM-Xe, $^{129}Xe_{rad}$, $^{131-136}Xe_{244}$ from ^{244}Pu fission, $^{131-136}Xe_{238}$ from ^{238}U fission, and Air-Xe acquired either from sample contamination, during transport and emplacement in the lithosphere, or by earlier recycling from the atmosphere into mantle reservoirs [19–21,28,30]. Arbitrary values were initially assigned to four mixing ratios of these components: $(^{136}Xe_{238}+{}^{136}Xe_{244})/{}^{130}Xe_{PEM}$, $^{136}Xe_{238}/(^{136}Xe_{238}+{}^{136}Xe_{244})$, $^{129}Xe_{rad}/{}^{136}Xe_{244}$, and $^{130}Xe_{Air}/{}^{130}Xe_{PEM}$. Mixing ratios were then varied and the resulting calculated compositions compared to measured compositions. This was repeated until $\Sigma_i(\Delta/\sigma)_i^2$ summed over all isotope ratios was minimized, where Δ_i is the difference between the calculated and measured $^{i}Xe/^{130}Xe$ ratio and σ_i is the 1σ uncertainty in the difference.

Measured Xe compositions in CO_2 well gases [22] and MORB are listed in Table 1. The MORB data base [6] contains 38 isotopic compositions of Xe fractions

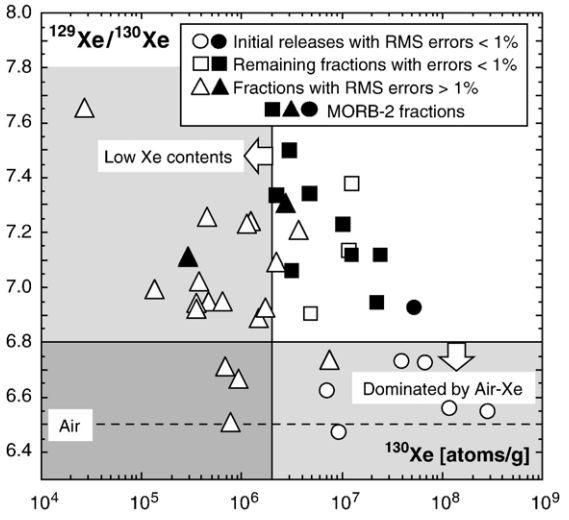

Fig. 1. $^{129}Xe/^{130}Xe$ vs. ^{130}Xe for the 38 MORB Xe release fractions [6]. Plotted compositions are categorized by their root-mean-square (RMS) measurement errors averaged across all isotope ratios; they exceed 1% in all fractions with ^{130}Xe contents $<2\times10^6$ atoms/g. Six of the 7 fractions initially released from the samples with RMS errors <1% are dominated by air contamination (>96% Air-Xe) and no plausible mixing ratios were obtained. Filled symbols identify the 11 fractions included in the MORB-2 average. Ten of these group in the upper right quadrant of the figure, and of the 11 only 2 have RMS errors >1%, illustrating the sensitivity of the minimization procedure to measured data uncertainties.

evolved by stepwise pyrolysis or crushing from 11 samples taken from 6 MORB rocks. Many degassing steps released only small amounts of Xe with large measurement uncertainties, so the data appeared to have limited usefulness (e.g. [8,31]). On closer examination, however, they tell a consistent story. The complete MORB data set is illustrated in Fig. 1, where measurements with higher Xe abundances and less atmospheric contamination fall in the upper right quadrant. Two different but overlapping data subsets, using slightly different selection criteria and composed primarily of measurements in this quadrant, yielded physically realistic mixing ratios of the components. These were used to derive the "Average MORB-1" and "Average MORB-2" compositions in Table 1. Details of data analyses, data filtering, and error estimates are given in the Appendix.

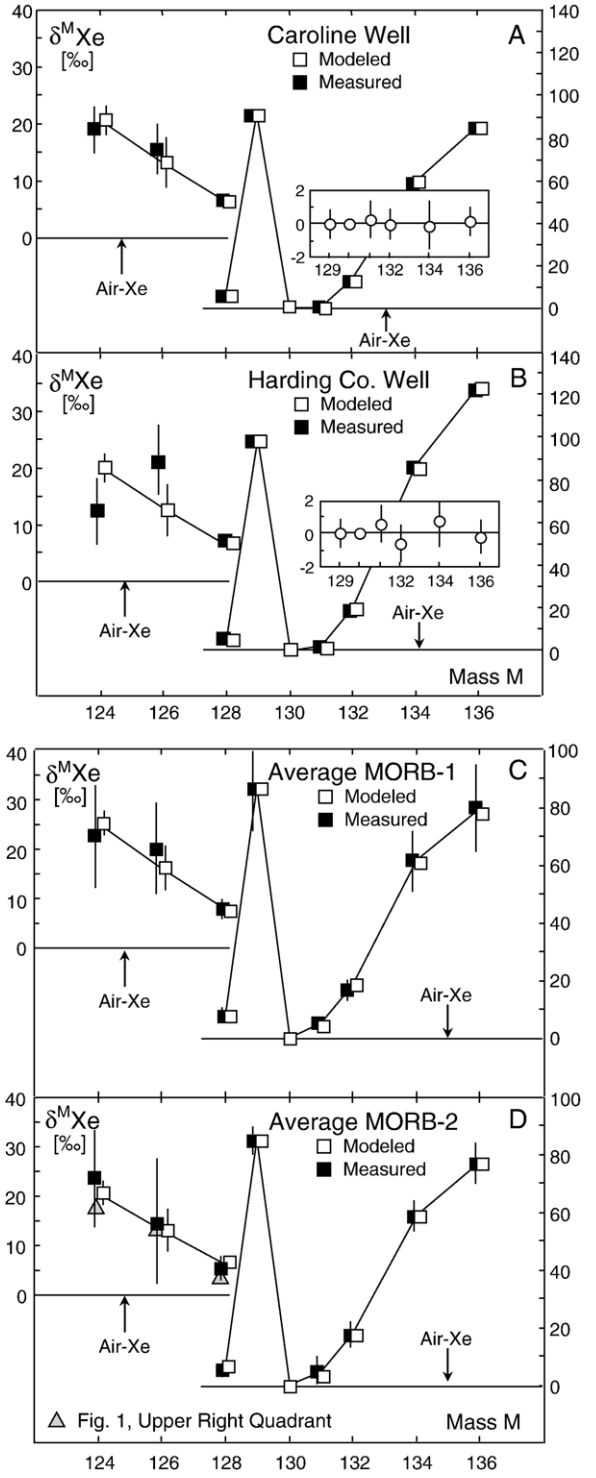

Fig. 2. Comparisons of measured ([22], Table 1) and modeled Xe isotopic distributions for the Caroline (A) and Harding County (B) gas wells, and for MORB-1 (C) and MORB-2 (D). Calculated compositions assume U–Xe as the PEM component; similarly good fits are obtained using either SW-Xe or Xe-Q. Data are plotted as permil (‰) deviations of $^{M}Xe/^{130}Xe$ ratios from the corresponding ratios in Air-Xe. Offsets between modeled and measured $^{129-136}Xe/^{130}Xe$ ratios (right scales) are too small to be visible in (A, B); they are shown in the insets in units of ‰ differences. Light-isotope ratios are shown at higher resolution (left scales). Shaded triangles in (D) are the ratios obtained by integrating all 15 fractions falling in the upper right quadrant of Fig. 1.

3. Solar-type nonradiogenic xenon in the mantle

Calculated component mixing solutions for well gas and MORB compositions are seen in Fig. 2 to be close matches to the measurements, supporting the assumption of simple component mixtures. Note that the measured $^{124,126,128}Xe/^{130}Xe$ ratios –involving isotopes containing no radiogenic or fissiogenic components– are clearly enhanced relative to Air-Xe in both the gas-well and MORB samples. Caffee et al. [22] established this light-isotope enrichment pattern in the well gases and discussed its implications for the PEM composition (which they assumed to be SW–Xe). A similar pattern has not been seen previously in MORB, where uncertainties in measurements of these low-abundance isotopes have generally been too large to rule for or against its presence. Here, however, the measured MORB ratios in Fig. 2C, D indicate small enrichments that trend coherently with mass, pointing to a PEM-Xe component that is neither Air-Xe nor NEA-Xe but instead is enhanced in the light isotopes relative to air — a characteristic shared by the "solar-type" U–Xe, SW–Xe, and meteoritic Xe–Q compositions (Table 1).

The identity of nonradiogenic PEM-Xe in the upper mantle clearly hinges on the reality of these small light-isotope elevations. Air-Xe and NEA-Xe are suitable PEM

components only if they are absent (as assumed by [6]). However this is unlikely unless an unrecognized analytic artifact is present in the measurements. The elevations are consistently present, at about the same magnitudes, in all higher-precision subsets of the data base –the three in Table 1, the integrated compositions of all 15 fractions in the upper right quadrant of Fig. 1 (plotted in Fig. 2D) and the 12 most precise measurements (<1% RMS errors) in that quadrant– and also in an expanded subset comprising ~75% of the 38 individual fractions (Appendix). Almost all are significant at the 1σ level, many at $\geq 2\sigma$, and display approximately the same declining pattern with increasing isotope mass as the solar-type compositions. Moreover there is evidence, discussed in Section 7, for correlated enrichments of ^{124}Xe, ^{126}Xe, and ^{129}Xe in *individual* fractions from the Xe-rich MORB rock 2ΠD43. These light-isotope elevations thus warrant exploration of the consequences of a solar-type Xe component in the MORB source. The observation that the elevations in Fig. 2 are much smaller than in the solar-type compositions in Table 1 indicates that a substantial air component is mixed with PEM-Xe in the samples, as previously concluded for the well gases [22,32].

4. Component mixtures and comparisons between MORB, well-gas, and atmospheric Xe

Mixing ratios and uncertainties (Appendix) yielded by minimization are given in Table 2 for U–Xe and SW-Xe as PEM components. Xe-Q generates the same values, within error, as SW-Xe. They were derived using MORB-2, our preferred MORB composition because the individual release fractions defining it all have minimization solutions, but using MORB-1 instead gives essentially the same results.

Air contamination comprises >90% of the ^{130}Xe inventories in Caroline, Harding Co., and MORB-2; air percentages in the 11 individual MORB-2 fractions range from 74% to 99%. The proportion of excess fission-generated ^{136}Xe that is plutogenic depends upon whether U–Xe or SW-Xe is used for PEM-Xe, a consequence of their distinct $^{134-136}$Xe/^{130}Xe ratios, but there is essentially no difference for $^{129}Xe_{rad}$. Resulting $^{129}Xe_{rad}/^{136}Xe_{244}$ ratios thus differ for the two PEM choices —modestly for MORB but substantially for the well gases.

4.1. Comparisons with previous results

Pu-derived fractions of total well-gas fission Xe obtained here (Table 2) agree within error with those reported by [22]. Component analysis of an earlier measurement of Harding Co. Xe [32] yields plutogenic Xe fractions very similar to the Table 2 values. An analysis of the MORB data by Kunz et al. [6] gave a fraction of Pu-derived ^{136}Xe in the fission excesses, relative to Air-Xe, of 32±10%. The substantially higher Pu–Xe fractions of 63–75% in Table 2 were derived with nonradiogenic mantle Xe taken to be U–Xe or SW-Xe instead of Air-Xe. The MORB composition used is the same, within uncertainties (Appendix, Table 1), and our minimization analysis, using Air-Xe, gives a comparably small Pu-Xe fraction (34%). The difference between the Kunz et al. and Table 2 results is therefore due primarily to different choices for PEM-Xe, not to disagreement in the composition of MORB Xe or the use of differing statistical methods.

Table 2
Modeling results for the average MORB-2, Caroline, and Harding Co. Xe compositions (Table 1), with two assumed compositions, U–Xe and SW-Xe, for Xe in the PEM (*P*rimordial *E*arth *M*antle)

Mantle reservoir =	MORB-2	Caroline	Harding Co.	MORB-2	Caroline	Harding Co.
PEM-Xe =	U–Xe	U–Xe	U–Xe	SW-Xe	SW-Xe	SW-Xe
% Air-Xe at ^{130}Xe	$92.0^{+0.7}_{-1.2}$	$91.90^{+0.50}_{-0.38}$	$92.06^{+0.50}_{-0.48}$	$91.9^{+1.1}_{-0.5}$	$91.86^{+0.40}_{-0.37}$	$92.10^{+0.51}_{-0.65}$
% PEM-Xe at ^{130}Xe	$8.0^{-0.7}_{+1.2}$	$8.10^{-0.50}_{+0.38}$	$7.94^{-0.50}_{+0.48}$	$8.1^{-1.1}_{+0.5}$	$8.14^{-0.40}_{+0.37}$	$7.90^{-0.51}_{+0.65}$
$^{136}Xe_{fission}/^{130}Xe_{PEM}$	$2.60^{+0.20}_{-0.25}$	$2.80^{+0.17}_{-0.10}$	$3.91^{+0.25}_{-0.23}$	$2.46^{+0.32}_{-0.31}$	$2.66^{+0.13}_{-0.09}$	$3.79^{+0.25}_{-0.25}$
% $^{136}Xe_{fission}$ from $^{238}U_{sf}$	37^{+19}_{-14}	$95.8^{+1.3}_{-3.1}$	$96.2^{+1.7}_{-1.8}$	25^{+21}_{-11}	$87.8^{+2.0}_{-3.5}$	$91.8^{+2.3}_{-2.9}$
% $^{136}Xe_{fission}$ from $^{244}Pu_{sf}$	63^{-19}_{+14}	$4.2^{-1.3}_{+3.1}$	$3.8^{-1.7}_{+1.8}$	75^{-21}_{+11}	$12.2^{-2.0}_{+3.5}$	$8.2^{-2.3}_{+2.9}$
$[^{129}Xe_{PEM}+^{129}Xe_{rad}]/^{130}Xe_{PEM}$	$13.37^{+0.79}_{-0.46}$(a)	$13.83^{+0.42}_{-0.34}$(b)	$14.64^{+0.68}_{-0.45}$(b)	$13.35^{+0.99}_{-0.44}$	$13.79^{+0.30}_{-0.28}$	$14.68^{+0.95}_{-0.56}$
$[^{136}Xe_{PEM}+^{136}Xe_{244}]/^{130}Xe_{PEM}$	$3.29^{+0.23}_{-0.44}$(a)	$1.77^{+0.07}_{-0.04}$(b)	$1.80^{+0.06}_{-0.06}$(b)	$3.64^{+0.26}_{-0.53}$	$2.12^{+0.07}_{-0.05}$	$2.11^{+0.08}_{-0.08}$
$^{129}Xe_{rad}/^{136}Xe_{244}$	$4.3^{+1.9}_{-0.7}$	64^{+35}_{-26}	56^{+42}_{-17}	$3.8^{+2.0}_{-0.4}$	$23.2^{+5.2}_{-4.8}$	27^{+14}_{-6}
Xe–Xe closure age [Ma](c)	96^{+5}_{-10}	20^{+15}_{-12}	24^{+11}_{-15}	100^{+3}_{-12}	$49.1^{+6.9}_{-5.5}$	45^{+8}_{-11}

(a) $MORB_p$ compositions (Fig. 4).
(b) $Caroline_p$ and $Harding\ County_p$ compositions (Fig. 6).
(c) Closure ages from Eq. (1), with ^{238}U (BSE)=21 ppb, ^{127}I (BSE)=13 ppb, $(^{238}U/^{127}I)_o$=1.75, $(^{244}Pu/^{138}U)_o=6.8\times10^{-3}$ [43], and $(^{129}I/^{127}I)_o=1.1\times10^{-4}$ [44].

4.2. MORB–well gas comparisons

Similarities in the compositions of MORB and well-gas Xe have been used to argue that both derive from the same mantle reservoir (e.g. [33,8]). As seen in Table 1 and Fig. 2, measured compositions are indeed not very different, particularly for masses below ^{129}Xe, and correspondences in calculated ^{129}Xe/^{130}Xe and Air/PEM mixing ratios, reflected in similar $^{124-128}$Xe/^{130}Xe ratios (Fig. 2), are evident in Table 2. Moreover, Ne compositions [22] and ^{40}Ar/^{36}Ar [34] in the well gases are MORB-like, and although ^{3}He/^{4}He ratios are lower [22], this could be due to addition of crustal radiogenic ^{4}He to the well gases.

A central result of the present analysis, however, points to a serious problem with a common source: $^{129}Xe_{rad}$/$^{136}Xe_{244}$ ratios in MORB are strikingly *dissimilar* to those in the well gases, nominally lower by factors of ~14 (U–Xe base) to ~7 (SW-Xe). These differences are much larger than uncertainties due to measurement errors. Extreme minimum $^{129}Xe_{rad}$/$^{136}Xe_{244}$ values obtained in 30 solutions using input Caroline compositions that were randomly varied within their 1σ measurement errors (Appendix) were still factors of ~6 to ~3 higher than the MORB ratios; essentially the same differences were obtained with a corresponding perturbation of the MORB data. The higher ratios in the well gases result from their much lower proportions of plutogenic to uranogenic Xe; analyses here and in [22] indicate that most (≥85%) of the fission Xe in Caroline and Harding Co. is from ^{238}U. Nevertheless the high measurement accuracy attained by [22] allows relatively precise isolation of Pu-derived Xe.

4.3. MORB–atmosphere comparisons

The $^{129}Xe_{rad}$/$^{136}Xe_{244}$ ratios derived for MORB in this analysis are $4.3^{+1.9}_{-0.7}$ with a U–Xe base composition and $3.8^{+2.0}_{-0.4}$ with a SW-Xe base (Table 2). The corresponding ratio for the atmosphere, with a nonradiogenic NEA-Xe base, is 4.36±0.43 [16]. MORB and atmospheric values are indistinguishable within uncertainties for either choice of nonradiogenic PEM-Xe, another key result of this study; for the U–Xe base, they are nominally identical. Implications of this agreement for relationships between the atmospheric and MORB reservoirs and for MORB degassing chronologies are discussed in Section 8.

5. Reservoir closure ages

The $^{129}Xe_{rad}$/$^{136}Xe_{244}$ ratios can be used to constrain the timing of Xe loss from a reservoir. Assuming efficient loss of Xe from a mantle reservoir up to a "closure age" T, and subsequent complete retention of ^{129}I and ^{244}Pu decay products, the amount of radiogenic $^{129}Xe_{rad}$ now present is $^{129}Xe_{rad} = {}^{129}I_o e^{-\lambda_{129}T} = {}^{127}I_o\left(\frac{^{129}I}{^{127}I}\right)_o e^{-\lambda_{129}T}$, where $^{127}I_o$ is the abundance of stable iodine and $(^{129}I/^{127}I)_o$ the ratio of radioactive ^{129}I to ^{127}I at solar-system origin 4567 Ma ago [4]. Accumulated ^{136}Xe from ^{244}Pu decay is $^{136}Xe_{244} = {}^{136}Y_{244}Pu_o e^{-\lambda_{244}T} = {}^{136}Y_{244}U_o\left(\frac{^{244}Pu}{^{238}U}\right)_o e^{-\lambda_{244}T}$, where $^{238}U_o$ and $(^{244}Pu/^{238}U)_o$ are respectively the uranium abundance and Pu/U ratio in Earth-forming materials at 4567 Ma and $^{136}Y_{244}$ is the yield of ^{136}Xe atoms per ^{244}Pu decay. Combining these two equations [5] yields the Xe–Xe closure age of the reservoir, which depends only on abundance ratios:

$$T = \frac{1}{\lambda_{244}-\lambda_{129}} \times \ell n\left[\frac{(^{129}Xe_{rad}/^{136}Xe_{244})(^{238}U/^{127}I)_o(^{244}Pu/^{238}U)_o\,{}^{136}Y_{244}}{(^{129}I/^{127}I)_o}\right]. \quad (1)$$

For two Xe reservoirs, their difference in closure age is

$$\Delta T = T_1 - T_2 = \frac{1}{\lambda_{244}-\lambda_{129}}\ell n\left[\frac{(^{129}Xe_{rad}/^{136}Xe_{244})_1(^{238}U/^{127}I)_{o,1}}{(^{129}Xe_{rad}/^{136}Xe_{244})_2(^{238}U/^{127}I)_{o,2}}\right]. \quad (2)$$

This is independent of initial $(^{244}Pu/^{238}U)_o$ and $(^{129}I/^{127}I)_o$, and if both reservoirs evolved with a common U/I, ΔT depends only on their present $^{129}Xe_{rad}$/$^{136}Xe_{244}$ ratios.

Closure ages of noble gas reservoirs from Eq. (1) are plotted in Fig. 3 as functions of mantle U/I ratio for two possible reservoir PEM-Xe compositions. Filled symbols assume a nominal U/I ratio, corrected for uranium decay, calculated from best-estimate uranium and iodine abundances in the present bulk silicate Earth. While the BSE uranium abundance seems well established, considerable uncertainty exists about iodine and therefore the U/I ratio, and so the plotted age lines represent Eq. (1) solutions for a wide range of mantle U/I. Data used in constructing Fig. 3 are given in the caption.

Atmospheric and MORB closure ages for nominal U/I fall between ~95 and 100 Ma, with differences ΔT nil within error. The ages remain in agreement, at various values, for any choice of U/I; they would differ only if this ratio in the atmospheric source was distinct from MORB (Eq. (2)). If the MORB and well gas sources evolved with same nominal U/I, the Caroline and Harding Co. reservoirs degassed between ~22 Ma and ~47 Ma, much earlier than the MORB-atmosphere

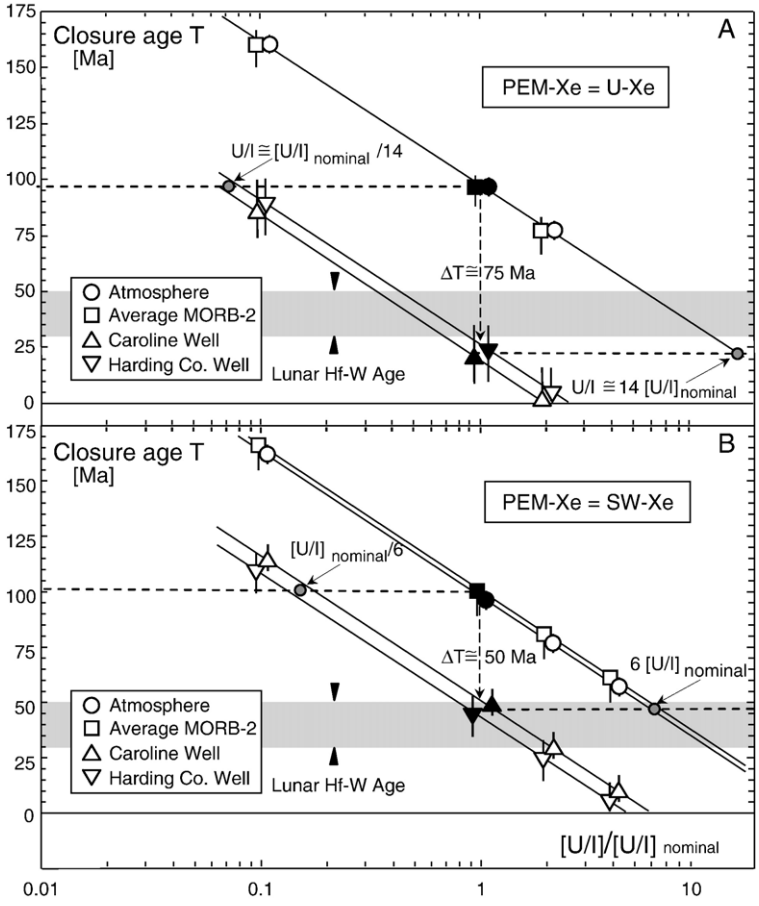

Fig. 3. Xe–Xe closure ages T from Eq. (1) for the atmosphere, MORB, and the Caroline and Harding Co. gas wells, with PEM-Xe = U–Xe (A) and SW-Xe (B). Xe-Q generates the same ages, within a few Ma, as SW-Xe. Filled symbols identify ages based on the best-estimate BSE abundances of $^{238}U \cong 21$ ppb and $^{127}I \cong 13$ ppb [8]; their ratio, corrected for uranium decay, is represented in the diagrams by $[U/I]_{nominal} = (^{238}U/^{127}I)_o$. The inclined lines represent solutions of Eq. (1) as functions of U/I, with fixed $^{129}Xe_{rad}/^{136}Xe_{244}$ ratios corresponding to each reservoir; open symbols are examples of ages calculated for specific non-nominal values of U/I. Intersections (small circles) of these lines with the horizontal dashed lines identify pairs of U/I values that yield the same closure ages for the MORB-atmosphere and Caroline–Harding Co. reservoirs —e.g., on the upper (96 Ma) dashed "isochron" in (A) $U/I = [U/I]_{nominal}$ for MORB and $U/I = [U/I]_{nominal}/14$ for the gas wells. ΔT (Eq. (2)) represents the age offsets between them if the same [U/I] ratio applies to both reservoirs. Eq. (1) parameters are $^{129}Xe_{rad}/^{136}Xe_{244} = 4.36$ for the atmosphere [16] and Table 2 values for MORB and the well gases, $\lambda_{129} = 4.42 \times 10^{-8}$ a^{-1} [42], $\lambda_{244} = 8.66 \times 10^{-9}$ a^{-1} [42], $^{136}Y_{244} = 7.0 \times 10^{-5}$ atoms/decay [42], $(^{244}Pu/^{238}U)_o = 6.8 \times 10^{-3}$ [43], $(^{129}I/^{127}I)_o = 1.1 \times 10^{-4}$ [44], and $(^{238}U/^{127}I)_o = 1.75$ (2.03 times the present ratio due to ^{238}U decay over 4567 Ma). Lunar Hf–W age range from [15]. The MORB closure ages in (A) and (B) are derived from the integrated MORB-2 composition, but MORB-1, Kunz et al. MORB, and other subsets of the data base, including averages of the individual fractions comprising MORB-1 and MORB-2, give similar values of $^{129}Xe_{rad}/^{136}Xe_{244}$, and closure ages consistent with the atmospheric age within their uncertainties.

system. The age differences ΔT between MORB and the well gases are constant for any value of U/I common to both reservoirs, and lie between ~75 and ~50 Ma depending on the assumed PEM component.

6. One degassing event, or two?

Diminishing the calculated ~75–50 Ma ΔT offsets in the well-gas and depleted mantle closures can be done only by assuming very different U/I ratios in different parts of the bulk silicate Earth. For example, as indicated by the dashed horizontal "isochron" lines in Fig. 3, both sources could have closed at ~95–100 Ma if an iodine-rich mantle reservoir that supplies the well gases was established very early with a U/I ratio lower than the nominal BSE value by factors of ~14 (Fig. 3A) to 6 (Fig. 3B). Alternatively, MORB-atmosphere closure in the well-gas age range would follow if iodine in the upper mantle MORB source was correspondingly depleted during a moon-forming collision, possibly accompanied by partial losses of moderately volatile species such as Rb, K, and Pb as discussed by [13].

There are no indications that moderately volatile elements vary dramatically within the mantle based on the limited range in U/Pb and Rb/Sr ratios inferred from Pb and Sr isotope compositions. Nevertheless it should be recognized that I is more volatile than either Pb or Rb, may be more likely to be atmophilic under thermal conditions prevailing in the upper mantle and atmosphere following a giant impact [35], and so could have been preferentially entrained and lost in post-impact hydrodynamic outflow. Iodine could escape with about the same efficiency as Xe, as discussed in a similar scenario for Mars [17].

The timing of a moon-forming collision on Earth has been calculated from terrestrial and lunar ^{182}W excesses generated by decay of ^{182}Hf ($\tau_{1/2}$=8.9 Ma) to be somewhere between ~25 and 30 Ma [10–12], lower limits of ~40–50 Ma [13,14], and 40±10 Ma [15] after solar-system formation. In view of the uncertainties in PEM-Xe compositions and U/I ratios, and the assumption of abrupt and complete reservoir degassing underlying Eq. (1), it is unclear how seriously the closure ages calculated here can be taken as accurate measures of degassing timing. However it is interesting that the well-gas reservoirs, characterized by either of two plausible primordial Xe compositions and a best-estimate U/I ratio for the BSE, have closure ages of ~20–50 Ma, in the neighborhood of Hf–W estimates for the giant impact. Such an impact could account for the substantial losses from deep interior reservoirs required by Xe isotopes, and would drive atmospheric losses.

The MORB-atmosphere system could have closed in the same time range as the well gas source *if* the impact depleted MORB iodine by factors of ~6–14 relative to the nominal 13 ppb (Fig. 3) — i.e., to ~1–2 ppb. It could simultaneously have degassed the uppermost mantle more severely than deeper regions, as required by the ~20-fold lower PEM-Xe abundance in the MORB source compared to the well gas reservoir (Section 7). The alternative is a second large-scale impact at ~95–100 Ma that degassed just the upper mantle. Without geochemical evidence that MORB iodine following the moon-forming collision could have been as low as ~1–2 ppb, a reasonable working hypothesis is that U/I in both interior reservoirs is approximately the best-estimate BSE ratio, and thus that two degassing events have been recorded. Only the calculated timing of MORB-atmosphere closure is significantly dependent on this assumption. Mixing ratio derivations are independent of chemical compositions, and so the MORB and gas-well ratios in Table 2, and their differences, are unaltered for any choice of U/I.

"Degassing" or "loss" events are taken here to be large impacts, not interior processes such as core formation or thermally driven differentiations that deposit volatiles in the atmosphere, because outgassed Xe decay products (and missing I, if such depletions occurred) must be lost *from the planet*. Atmospheric escape powered by impacts or other inputs of external energy can do this, and also fractionate the residual atmosphere; interior degassing mechanisms cannot. However combination of the two is possible, perhaps likely —degassing by interior processes and later atmospheric removal driven by collision or solar ultraviolet radiation.

7. Isotopic evolution of the MORB and gas-well reservoirs

7.1. MORB

Possible evolution paths for the mantle reservoir that supplied MORB gases are shown in Fig. 4. Prior to the degassing event the amounts of nonradiogenic nuclides were sufficiently high that Xe did not evolve isotopically. Most of the radiogenic isotopes that had been produced are then lost, as is most of the nonradiogenic Xe, so ^{129}I/^{130}Xe and ^{244}Pu/^{130}Xe ratios are greatly increased. Evolution from nonradiogenic U–Xe then follows the Stage I trajectory as the $^{129}Xe_{rad}$ and $^{136}Xe_{244}$ decay products accumulate in a closed reservoir, reaching the composition called MORB$_p$ ≥350 Ma later when ^{129}I and ^{244}Pu were essentially extinct. The MORB$_p$ point and its uncertainties (Table 2) represent the post-decay composition of MORB Xe at these isotopes without the air and ^{238}U fission components. Stage II evolution from MORB$_p$ reflects addition of ^{238}U fission Xe. Mantle ratios are then driven down the Stage III line by addition of Air-Xe. The MORB$_p$ and terminal Stage II compositions are derived by minimization using MORB-2 input data, and the modeled Stage III is simply a line drawn from the latter to air. For modeling consistency the individual MORB-2 fractions must lie along that line. This requirement is met: the dashed Stage III trajectory in Fig. 4, derived from correlation analysis of the MORB-2 data plotted in the inset, passes precisely through both the Stage II terminus and Air-Xe.

NEA-Xe and Air-Xe in Fig. 4 are connected by a line with slope equal to the atmospheric $^{129}Xe_{rad}/^{136}Xe_{244}$ ratio of 4.36. The line from U–Xe, drawn with this same slope, crosses MORB$_p$ essentially at its nominal composition. The MORB source and the atmosphere thus appear to contain very nearly the same ratio of Xe decay products. They have evolved, however, from different nonradiogenic base compositions, the former by addition of radiogenic and plutogenic components to U–Xe in an isolated interior reservoir and the latter by degassing

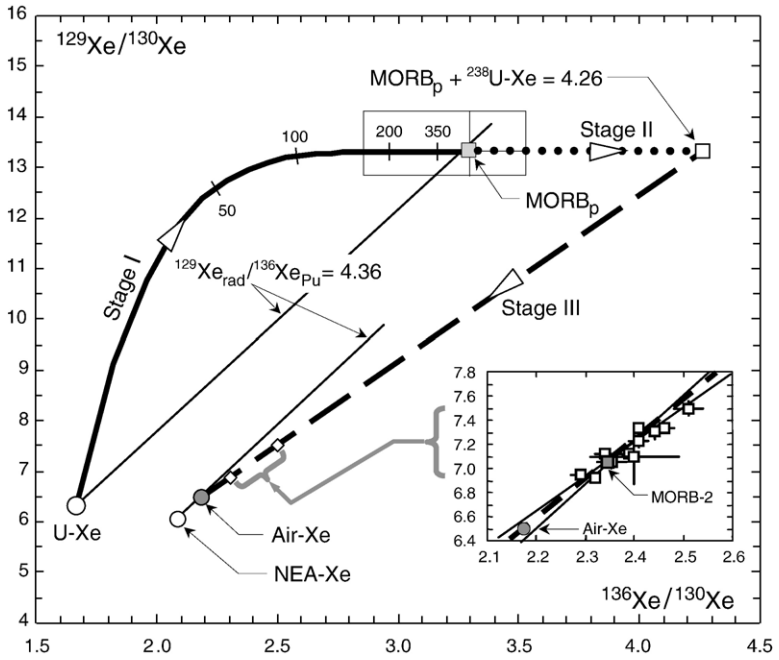

Fig. 4. Evolution of MORB $^{129}Xe/^{130}Xe$ and $^{136}Xe/^{130}Xe$ ratios. Starting from nonradiogenic PEM Xe, here taken as U–Xe, $^{129}Xe_{rad}$ and $^{136}Xe_{244}$ accumulate during Stage I evolution in an isolated mantle reservoir. Elapsed times in Ma following reservoir degassing and subsequent closure indicated by labeled ticks. Closure and commencement of isotopic evolution occurs at ~95 Ma if the MORB source has the nominal U/I ratio (Fig. 3). After a further ≥350 Ma, when ^{129}I and ^{244}Pu have mostly decayed, the reservoir approaches a final composition called $MORB_p$, defined by the mixing ratios identified in Table 2. Replicating this composition by adding decay products to nonradiogenic U–Xe requires 1.4×10^7 atoms/g of U–^{130}Xe in the MORB reservoir. Stage II represents addition to $MORB_p$ of Xe generated by fission of ^{238}U; evolution is horizontal since fission produces little ^{129}Xe. At the end of Stage II, $^{136}Xe/^{130}Xe=4.26$ ($^{136}Xe/^{130}Xe$ in U–Xe (Table 1) plus $^{136}Xe_{fission}/^{130}Xe_{PEM}$ (Table 2)); this would be the present-day ratio in MORB in the absence of air contamination. In Stage III, Air-Xe is added to the terminal Stage II composition. The 11 MORB-2 fractions and their summed composition (Table 1) are shown in the inset. The dashed-line correlation of the individual fractions, from York's [37] least-squares fitting algorithm, is plotted as the dashed Stage III trajectory in the main diagram. It coincides with the predicted line from the Stage II terminus to Air-Xe, and has the same slope within error (3.26±0.39) as the fit to all the MORB data [6]. $MORB_p$ compositions separately calculated for SW-Xe (Table 2) and Xe-Q as nonradiogenic base components agree within error. If either is used instead of U–Xe, the interpretations discussed in the text remain valid within the $MORB_p$ uncertainties. This is also the case if the ±10% uncertainty in atmospheric $^{129}Xe_{rad}/^{136}Xe_{244}$ is taken into account.

from the source reservoir to an atmosphere containing escape-fractionated U–Xe (NEA-Xe).

MORB mixing ratios in Table 2, derived assuming solar-type PEM-Xe in the source and consequently requiring a large air component, are not necessarily unique. The small observed light-isotope elevations (Fig. 2C, D) result from Air-Xe dilution of the much higher $^{124-128}Xe/^{130}Xe$ ratios in solar-type Xe. But they might instead reflect low ratios in the PEM component itself, produced for example by mixtures of indigenous U–Xe or SW-Xe with atmospheric NEA-Xe convectively transported into the MORB reservoir following the impact event. The PEM composition then lies on the U–NEA line in Fig. 4. Minimization solutions using such mixtures and MORB-2 data result in more PEM-Xe in the reservoir, lower isotope ratios for the $MORB_p$ and terminal Stage II compositions compared to Fig. 4 values, and less Air-Xe as NEA-Xe partly substitutes for it. In particular, for PEM mixtures of U–Xe and NEA-Xe, $^{129}Xe/^{130}Xe$ in $MORB_p$ is <13.37, reaching a minimum for 85% NEA-Xe at ~7.50, the highest measured ratio (which in this extreme case is air-free) in the MORB-2 data set (Fig. 4 inset). However $^{129}Xe_{rad}/^{136}Xe_{244}$ ratios and closure ages are unaltered from the pure U–Xe case –a 4.36 line from PEM still passes through $MORB_p$– and Fig. 2D is unchanged.

Modeling based on the presence of a solar-type PEM component predicts Stage III correlations, as in the Fig. 4 inset, involving isotopes *not* containing Xe decay products. The best chance to observe these is in the Xe-rich 2ΠD43 "popping rock" [36], considered to "bear the most pristine sampling of upper-mantle volatiles" [6]. A plot of nonradiogenic $^{124}Xe/^{130}Xe$ vs. $^{129}Xe/^{130}Xe$ in individual MORB-2 fractions from 2ΠD43 and their best-fit correlation [37] is shown in Fig. 5A. Transferred to the Fig. 5B evolution diagram for

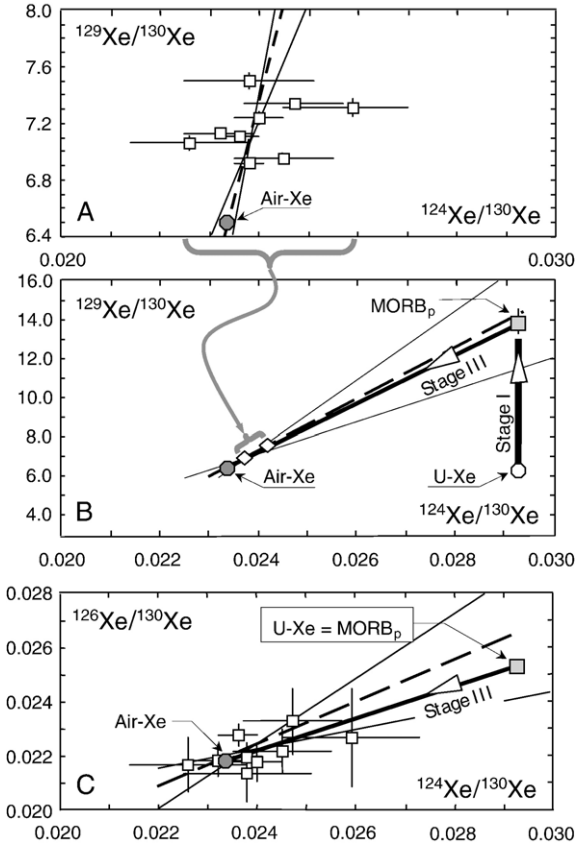

Fig. 5. Evolution of $^{124}Xe/^{130}Xe$ vs. $^{129}Xe/^{130}Xe$, and $^{124}Xe/^{130}Xe$ vs. $^{126}Xe/^{130}Xe$, in MORB rock 2ΠD43. Ten of the 11 MORB-2 fractions are from 2ΠD43. Nine of these 10 are plotted in (A), where the least-squares linear fit [37] is shown by the heavy dashed line, and its associated error envelope by lighter lines. The 10th fraction, 2ΠD43#6, 400× [6], has a $^{124}Xe/^{130}Xe$ uncertainty that spans the width of the plot; since the York fitting routine [37] weights the data points by the inverse squares of measurement errors, this datum has little influence on the correlation and is omitted. The diagram in (B) is similar to Fig. 4, except that for these isotopes only $^{129}Xe_{rad}$ is added by decay and so Stage I evolution from U–Xe to $MORB_p$ is vertical, and the isotope ratios are unchanged in Stage II. Note that the solid line representing Stage III addition of Air-Xe to the $MORB_p$ composition is closely replicated by the dashed correlation line from (A). The $^{129}Xe/^{130}Xe$ ratio for $MORB_p$ in (B) is that given by minimization analysis of the 9-fraction 2ΠD43 data set. It falls within the uncertainty of the Table 2 value derived from the full MORB-2 set. Panel (C) shows an analogous evolutionary diagram for ^{124}Xe and ^{126}Xe. Here isotope ratios are unaltered in both Stage I and Stage II, and thus the $MORB_p$ composition is U–Xe. The 9 fractions from 2ΠD43 yield a York correlation (dashed line) which, while not as close a match as in (B), is still consistent within its error envelope with Stage III air addition to $MORB_p$.

these isotopes, this correlation line is seen to be consistent with the requirement that the data fall along the Stage III trajectory from $MORB_p$ to Air-Xe. This is also the case, although with greater divergence, for the ^{124}Xe and ^{126}Xe isotope pair in Fig. 5C. Both fits pass directly through Air-Xe, as required, and Fig. 5A indicates that light-isotope variations do appear to correlate with radiogenic excesses, despite a statement to the contrary by [6]. While these correlations are not robust –data scatter and measurement uncertainties are considerable, and the error envelopes generated by the fitting procedure are large– they nevertheless are further indications that the light-isotope elevations in the integrated MORB compositions (Fig. 2C, D) are real.

7.2. Caroline and Harding County

Evolution of Xe in the reservoirs supplying the well gases is shown in Fig. 6 with U–Xe as the starting composition. After impact degassing the source isotope ratios evolve through Stage I to the post-decay *p*-compositions identified in Table 2. These compositions are very similar for Caroline (S. Australia) and Harding Co. (New Mexico), and so are consistent with Xe evolved from an isotopically uniform source. The wide geographic separation of the two sites suggests that this reservoir is globally distributed [22].

Since accumulation of daughter nuclides either commenced earlier than in the MORB source or the iodine abundance was higher, initial $^{129}I/^{244}Pu$ abundance ratios were much larger, and these compositions have correspondingly higher ratios of radiogenic to plutogenic components (~60 in Fig. 6) as seen in the Table 2 ratios. Required PEM-Xe abundances are also ~20–25 times higher than in the MORB source (Figs. 4 and 6 captions). The large ^{238}U fission Xe components driving Stage II evolution far to the right likely reflect crustal contamination.

8. Implications of similar $^{129}Xe_{rad}/^{136}Xe_{244}$ ratios in MORB and the atmosphere

Two possibilities exist for the relationship between the atmosphere and an upper mantle reservoir with identical $^{129}Xe_{rad}/^{136}Xe_{244}$ ratios. The first is delayed outgassing. After impact-driven losses from the mantle and atmosphere, mantle Xe evolved along the Stage I trajectory in Fig. 4 without significant degassing. After ~350 Ma, when little ^{244}Pu remained and the $MORB_p$ composition was reached, Xe outgassed to the atmosphere on an undefined time scale. Atmospheric Xe and residual Xe in the mantle source would then have the same composition since separation occurred after the parent isotopes were no longer present.

Delayed outgassing requires a sustained post-impact period of upper mantle quiescence. The second

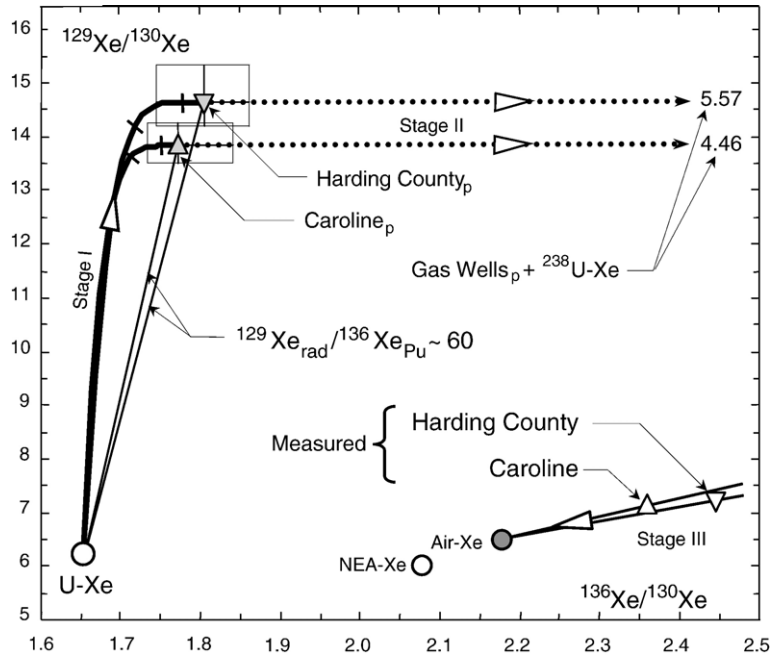

Fig. 6. Analogous to Fig. 4, but here for evolution of $^{129}Xe/^{130}Xe$ and $^{136}Xe/^{130}Xe$ from U–Xe in the Caroline and Harding Co. gas well reservoirs. See Fig. 4 caption for Stage and *p*-composition definitions. Reservoir closures for nominal U/I occur at 20 Ma for Caroline and 24 Ma for Harding Co., or at 49 and 45 Ma respectively if SW-Xe is the base composition (Table 2, Fig. 3). Ticks on the Stage I growth curves indicate ratio values 100 and 200 Ma after closures. The Caroline$_p$ and Harding County$_p$ compositions (Table 2) are reached ~150 Ma later; required reservoir abundances of U–^{130}Xe are 3.7×10^8 atoms/g for Caroline and 2.8×10^8 atoms/g for Harding Co. The large ^{238}U fission components in the well gases drive the terminal Stage II compositions far off scale to the right. The end of Stage III evolution from these compositions to measured ratios by air addition is shown at the lower right.

possibility assumes the opposite —that the upper part of the mantle layer affected by the impact was convecting vigorously enough during the following >350 Ma to continually release radiogenic and fissiogenic Xe, and ultimately degassed completely so that all the radiogenic isotopes produced there are now in the atmosphere. In the meantime Xe in an isolated deeper section of this layer grew to the MORB$_p$ composition. The gases now found in the MORB source were subsequently introduced from this reservoir, and could also have contributed to the atmosphere.

An important characteristic of both scenarios is that the isotopic composition of MORB does not give a detailed degassing chronology. In the first, degassing is only constrained to occur ~350 Ma or more after the impact that expelled most of the volatiles from the upper mantle, in contrast to earlier views that Xe isotopes require very early degassing. In the second, MORB Xe is unrelated to atmospheric Xe, so no time information can be obtained by combining them. One well-known degassing model is built on the premise of substantial degassing driven by vigorous mantle convection within a few tens of Ma following the loss event [6]. If $^{129}Xe_{rad}/^{136}Xe_{244}$ in the atmosphere and MORB are equal, all such models, calling for degassing while the parent nuclides were still alive, are ruled out; the residual ratio in the source would then always be smaller than its value in the atmosphere due to the longer half life of ^{244}Pu (i.e., a greater fraction of ^{244}Pu than ^{129}I was still extant in the mantle after degassing [38]). While there is some error associated with the MORB ratio (Table 2), so that minor differences from the atmospheric ratio are possible, early degassing requires much larger differences.

Previous studies interpreted the higher $^{129}Xe/^{130}Xe$ ratio in MORB compared to the atmosphere (Table 1) to be due to early degassing, so that gases remaining in the mantle were supplemented by further decay of ^{129}I [39]. In our view this instead reflects a higher ratio of ^{129}I to ^{130}Xe in the source reservoir compared to the ratio of degassed $^{129}Xe_{rad}$ to ^{130}Xe in the atmosphere. Atmospheric $^{129}Xe_{rad}/^{130}Xe$ is lower because most of the nonradiogenic Xe in the atmosphere is unrelated to the mantle. It is primarily residual NEA-Xe generated by escape-fractionation of atmospheric U–Xe, and ^{130}Xe from this source is much larger than the amount degassed with $^{129}Xe_{rad}$ from the mantle. Abundances of degassed

PEM-Xe are also too small to significantly perturb the atmospheric NEA composition at the nonradiogenic isotopes.

9. Speculations on mantle reservoirs

A qualitative box diagram of inferred mantle reservoirs and degassing events is shown in Fig. 7. MORB and gas-well Xe appear to derive from distinct sources characterized by strongly differing $^{129}Xe_{rad}/^{136}Xe_{244}$ ratios (Table 2, Figs. 4 and 6). These reservoirs must have separated early and could reflect differing early degassing of the mantle with depth. A possibility for the gas-well source is early subducted ocean crust, since Nd isotope evidence indicates that this may be a significant trace element reservoir formed earlier than 4.5 Ga [40], though it is unclear how its formation would be related to the moon-forming event. Whatever its origin, the well gas reservoir is likely to have been stored at depth to avoid mixing and degassing in the upper mantle. It seems unlikely that the well gases are linked to the high $^{3}He/^{4}He$ OIB reservoir associated with mantle plumes, although

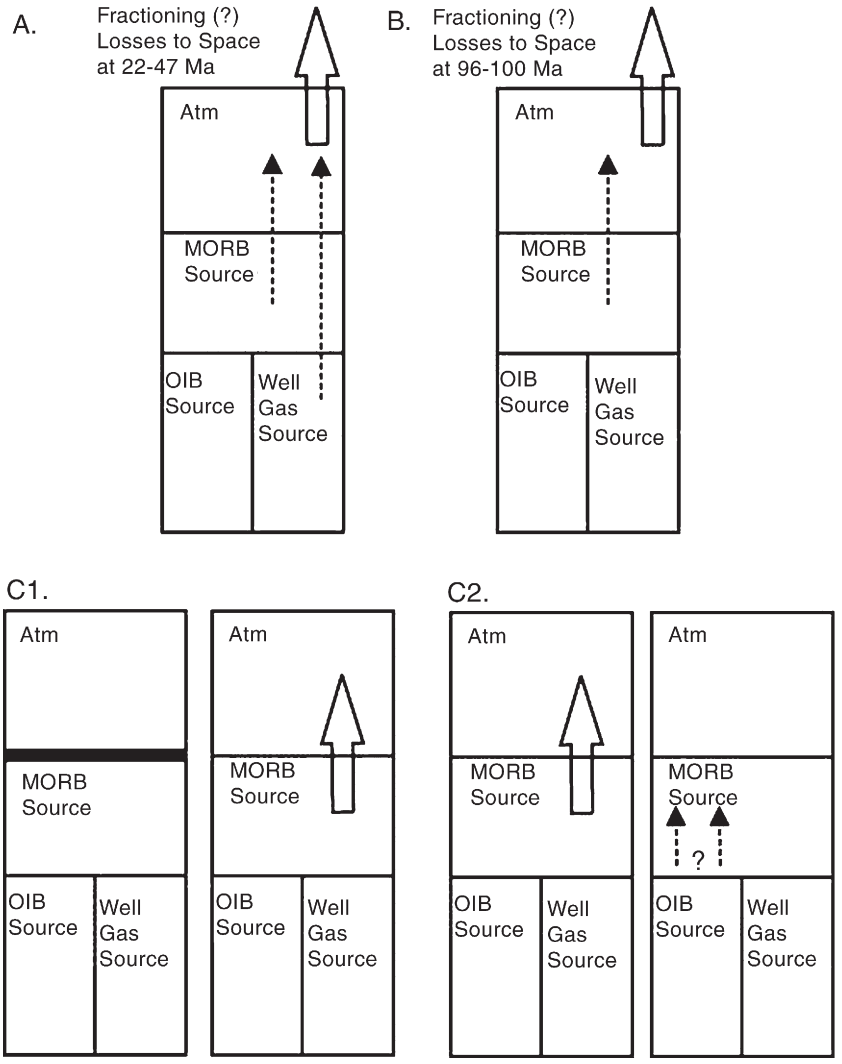

Fig. 7. A schematic of the sequence of degassing events assuming uniform U/I and thus two closure ages. An early loss event (A) is recorded in the well gas source, and must have affected the MORB source and atmosphere as well. A later loss event (B) did not affect the well gas source. Subsequently, there are two possibilities. If no degassing occurred until the parent nuclides had largely decayed away, radiogenic Xe in the atmosphere could then have degassed from the reservoir now sampled by MORB (C1). Alternatively, if the upper mantle continued to degas to the atmosphere following event B (C2), then it must have degassed completely, and the Xe now seen in MORB was derived from a deeper reservoir. Note that He isotopes suggest that there is a third reservoir supplying OIB. Its Xe characteristics, and so Xe evolution, are unknown. The geometries of the reservoirs are also unknown, and so the diagram is not meant to represent any particular configuration or relative reservoir volumes.

the lower well-gas $^{3}He/^{4}He$ [22] is not definitive evidence because of possible crustal ^{4}He contamination. OIB-Xe composition has not yet been clearly defined; however comparison of neon compositions argues against a common source for the OIB and well gases. Isotope ratios in well-gas Ne fall close to the MORB correlation [22], while Ne in OIB (e.g., Loihi) is clearly the product of a reservoir with a distinctly higher Ne/(U+Th) ratio [8]. Therefore a third noble gas reservoir is apparently needed to supply the well gases.

Long-term preservation of Xe isotope differences between the MORB and gas well reservoirs is an uncomfortable requirement, both because another isolated volatile storage site must be located, and because the well gases, apart from $^{129}Xe_{rad}/^{136}Xe_{244}$, are strikingly similar to MORB in noble gas characteristics. While the source of gas well Xe is likely in the deeper mantle, it is not clear exactly what the nature of this reservoir is nor how to isolate it from other mantle reservoirs. There is no evidence for the supply of well gases from a deep source, e.g. through a mantle plume, and so it is possible that they reside in heterogeneities within the upper mantle. This possibility can be evaluated once more data are available to assess the existence and extent of heterogeneity; so far, the MORB noble gas reservoir has been characterized using samples that come primarily from only one location [6]. However, in order to preserve such differences, a long-term storage site that preserves the heterogeneities is still required. Interestingly, while the Xe isotope signature of the well gases and MORB, reflecting early degassing histories, are different, the Ne isotope signatures, reflecting long-term degassing histories, are similar. This suggests that the well gas Xe isotope signature is decoupled from the light noble gases. A possibility is that well gas Xe is derived from a reservoir that is depleted in nonradiogenic noble gases, but can supply a significant component of early-produced Xe to a more extensive reservoir with MORB-like He. However, it is not clear how radiogenic Xe is separated from other radiogenic noble gases. The main obstacle to developing noble gas models compatible with geophysical observations has been in defining a separate high $^{3}He/^{4}He$ reservoir that supplies the ^{3}He found in MORB. This problem is now extended to yet another reservoir.

Apart from geophysical considerations, there are puzzling features of Xe compositions and abundances in the inferred mantle reservoirs. Similar light-isotope enhancements in gas well and MORB Xe (Fig. 2) imply similar ratios of contaminant Air-Xe to indigenous solar-type Xe; that this could result from post-eruptive air contamination in two such different kinds of sample seems suspiciously coincidental. Approximately equal $^{129}Xe/^{130}Xe$ ratios in MORB and the well gases (Table 2, Figs. 4 and 6) require that the ratios of trapped ^{130}Xe to ^{129}I remaining after reservoir closures were the same, even though, with the hypothesis of two impacts widely separated in time, the closure time of the gas well source is earlier by 3–5 half-lives of ^{129}I (note, however, that these ratios would differ if nonradiogenic Xe in the MORB source was a mixture of U–Xe and NEA-Xe (Section 7)). Similar ratios could perhaps be generated if a single impact drove prompt degassing of some fraction of the Xe in the BSE, followed by additional and proportional losses of both Xe and ^{129}I from just the uppermost mantle, a possibility discussed in Section 6. But there still seems to be no obvious process that would lead naturally to similar final $^{129}Xe/^{130}Xe$ ratios in the two reservoirs.

It should be emphasized that these difficulties in interpreting the Xe data do not negate the results produced here, which are based on straightforward statistical analyses of analytical data. Rather, the features that appear contradictory within the context of current models may be indicating that there are some fundamental aspects of noble gas evolution and mantle structure that remain unidentified.

10. Summary

The three principal analytic findings of this study are identification of nonatmospheric light Xe isotope ratios in MORB, relative MORB abundances of iodine- and plutonium-derived Xe that differ greatly from the well gases, and nominally identical ratios of these decay products in MORB and the atmosphere. The first, in conjunction with similar elevations of $^{124-128}Xe/^{130}Xe$ ratios in the well gases ([22], Fig. 2), establishes the presence of solar-like Xe in both reservoirs, and by itself would support a common MORB-well gas source. The second, however, points to separate reservoirs differing in closure age by ~50–75 Ma if both contain the same uranium/iodine ratio. The third shifts association of MORB radiogenic Xe from the well gases to the atmosphere, a key change in constraints on mantle reservoirs.

The affiliation of Xe in MORB and the geophysical and compositional implications of the proposed reservoirs clearly require further study. Nonetheless the conclusion that two distinct $^{129}Xe_{rad}/^{136}Xe_{244}$ ratios exist in Earth, one defined by Xe in the atmosphere as well as MORB and the other by Xe in well gases, appears robust. If the BSE is indeed characterized by a common U/I ratio, these differing ratios reflect two distinctly different mantle degassing ages, with the earlier age

range, commensurate with Hf–W estimates of the timing of the moon-forming impact, presumably stored in the deeper mantle.

These new observations regarding Xe isotope distributions place additional constraints on mantle noble gas models. The perplexing features noted above from comparisons between atmospheric, MORB, and well-gas Xe provide a challenge for understanding terrestrial noble gas evolution, and suggest that some fundamental aspect of mantle degassing is missing from our current understanding. This study makes no attempt to construct a model around these data, but rather only seeks to identify the constraints any successful model for terrestrial noble gas evolution must satisfy.

Acknowledgements

This work was supported in Minnesota by the NASA Cosmochemistry Program, Grant NAG5-11723. The manuscript was substantially improved by comments from K. Farley, R. Carlson, M. Caffee, and three anonymous reviewers.

Appendix A

Minimizations of $\Sigma_i(\Delta/\sigma)_i^2$ were carried out using Microsoft Excel SOLVER. Tests of the routine with artificial multicomponent mixtures yielded precise deconvolution of component inputs. Convergences to unique minima for the MORB Xe and gas well compositions listed in Table 1 were reproducible over wide ranges of arbitrarily chosen initial mixing ratios. Searches of mixing space revealed no other minima, specifically no well-gas minimum in the neighborhood of the MORB minimum, and vice versa.

This minimization procedure was applied to the abundance-weighted integrated compositions of each of the 11 analyzed MORB samples. Four of these, all with total $^{130}Xe < 3\times10^6$ atoms/g and correspondingly large measurement errors, yielded no solutions. In 6 of the remaining 7, excepting only 2ΠD43#4, large air releases in the initial degassing steps (Fig. 1) dominated the integrated compositions to the extent that other components could not be accurately resolved. These 7 generated consistent minimization solutions, with the PEM-Xe taken to be either U–Xe or SW-Xe, when initial releases (except from 2ΠD43 #4) were excluded from the sums. They include 21 of the 38 individual Xe fractions in the MORB data base [6]; of these, 15 fall in the upper right quadrant of Fig. 1. "Average MORB-1" in Table 1 is the average of these 7 integrated Xe compositions.

Minimization was also applied to each of the 38 individual compositions in the data base. Unique solutions with physically realistic mixing ratios were obtained in 11 cases, all included in MORB-1 [All 96-18, 1600 °C; 2ΠD43 #2, 1000 °C; 2ΠD43 #3, 16×, 100×; 2ΠD43 #4, 660 °C, 1000 °C; 2ΠD43 #5, 1000 °C; 2ΠD43 #6, 10×, 15x, 25×, 400×]. "Average MORB-2" (Table 1), the abundance-weighted average of these 11, is identical to "Average MORB-1" within error. Fifteen of the remaining 27 fractions had Xe contents $<2\times10^6$ atoms/g (Fig. 1) with large isotopic uncertainties; only one of the 11 MORB-2 fractions was in this category. Of these 27 failures, 2 contained very little Xe ($<2\times10^5$ atoms/g), 20 yielded unphysical solutions (negative fractions of ^{238}U fission Xe or negative closure ages), and the other 5 either did not converge to minima, or yielded fractions of Air-Xe or ^{238}U fission Xe approaching 100% and therefore failed to resolve PEM-Xe or Pu-Xe components.

Kunz et al. [6] used a 13-fraction subset of their data, selected on different criteria, for Pu-Xe analysis. Twelve of these fall in the upper right quadrant of Fig. 1. Eight are included in the 11 used to define MORB-2, and the averaged Xe compositions of the two are the same within error (Table 1). A virtually identical composition results from integration over a larger subset, comprising ~75% of the total data base in Fig. 1, which excludes only initial release fractions containing essentially no Xe or dominated by air contamination.

Uncertainties in $^{129-136}Xe/^{130}Xe$ ratios in Table 1 are abundance-weighted integrations of isotopic errors in the 11 individual fractions comprising MORB-2, and standard errors of the means of the 7 integrated samples averaged to define MORB-1. A different procedure was used to estimate uncertainties in the light $^{124-128}Xe/^{130}Xe$ ratios, which are simple two-component mixtures of Air-Xe and PEM-Xe. Minimization yields PEM/Air mixing ratios, and these define expected values of $^{124-128}Xe/^{130}Xe$ in each analyzed composition. Measured ratios scatter randomly around these predicted values, almost all (~90%) with $(\Delta/\sigma)_i < 1$. Errors for the MORB-1 and MORB-2 light-isotope ratios in Table 1 and Fig. 2 C, D are the RMS deviations of measured and expected ratios. This approach eliminates non-statistical isotopic scatter due to variations in PEM/Air mixing ratios.

Errors in measured MORB and gas-well isotope ratios are the dominant sources of uncertainties in the component mixing ratios yielded by the minimization procedure. Sensitivities to input data were estimated using a simple Monte Carlo approach in which each isotope ratio in a measured composition was altered by randomly adding or subtracting a randomly chosen

fraction of its 1σ error. SOLVER was then used to generate a minimized $\Sigma_i(\Delta/\sigma)_i^2$ solution and a corresponding set of parameter values for the modified composition. Statistically stable estimates of uncertainties imposed by input data fluctuations were obtained after 30–60 solutions for the perturbed MORB and well-gas data. These are the errors attached to the mixing ratios in Table 2.

Measured Xe compositions in this study are referenced to Air-Xe. Their stated analytic errors do not include the minor uncertainties in Air-Xe composition. Inclusion of these would moderately increase the small statistical errors reported for Caroline and Harding Co. [22].

References

[1] G.W. Wetherill, Formation of the Earth, Annu. Rev. Earth Planet. Sci. 18 (1990) 205–256.

[2] J.E. Chambers, G.W. Wetherill, Making the terrestrial planets: N-body integrations of planetary embryos in three dimensions, Icarus 136 (1998) 304–327.

[3] G.R. Stewart, Outstanding questions for the giant impact hypothesis, in: R.M. Canup, K. Righter (Eds.), Origin of the Earth and Moon, Univ. of Arizona Press, Tucson, 2000, pp. 217–223.

[4] G.W. Wetherill, Radiometric chronology of the early solar system, Annu. Rev. Nucl. Sci. 25 (1975) 283–328.

[5] R.O. Pepin, D. Phinney, The formation interval of the Earth, Lunar Sci., vol. VII, Lunar and Planetary Institute, Houston, 1976, pp. 682–684.

[6] J. Kunz, T. Staudacher, C.J. Allègre, Plutonium-fission xenon found in Earth's mantle, Science 280 (1998) 877–880.

[7] M. Ozima, F.A. Podosek, Formation age of the Earth from $^{129}I/^{127}I$ and $^{244}Pu/^{238}U$ systematics and the missing Xe, J. Geophys. Res. 104 (1999) 25493–25499.

[8] D. Porcelli, C.J. Ballentine, Models for the distribution of terrestrial noble gases and evolution of the atmosphere, in: D. Porcelli, C.J. Ballentine, R. Wieler (Eds.), Noble Gases in Geochemistry and Cosmochemistry, Rev. Mineral. Geochem., vol. 47, 2002, pp. 411–480.

[9] R.O. Pepin, D. Porcelli, Origin of noble gases in the terrestrial planets, in: D. Porcelli, C.J. Ballentine, R. Wieler (Eds.), Noble Gases in Geochemistry and Cosmochemistry, Rev. Mineral. Geochem., vol. 47, 2002, pp. 191–246.

[10] Q. Yin, S.B. Jacobsen, K. Yamashita, J. Blichert-Toft, P. Télouk, F. Albarède, A short timescale for terrestrial planet formation from Hf–W chronometry of meteorites, Nature 418 (2002) 949–952.

[11] T. Kleine, G. Münker, K. Mezger, H. Palme, Rapid accretion and early core formation on asteroids and the terrestrial planets from Hf–W chronometry, Nature 418 (2002) 952–955.

[12] K. Righter, C.K. Shearer, Magmatic fractionation of Hf and W: constraints on the timing of core formation and differentiation in the Moon and Mars, Geochim. Cosmochim. Acta 67 (2003) 2497–2507.

[13] A.N. Halliday, Mixing, volatile loss and compositional change during impact-driven accretion of the Earth, Nature 427 (2004) 505–509.

[14] T. Kleine, K. Mezger, H. Palme, C. Münker, The W isotope evolution of the bulk silicate Earth: constraints on the timing and mechanisms of core formation and accretion, Earth Planet. Sci. Lett. 228 (2004) 109–123.

[15] T. Kleine, H. Palme, K. Mezger, A.N. Halliday, Hf–W chronometry of lunar metals and the age and early differentiation of the Moon, Science 310 (2005) 1671–1674.

[16] R.O. Pepin, On the isotopic composition of primordial xenon in terrestrial planet atmospheres, Space Sci. Rev. 92 (2000) 371–395.

[17] R.O. Pepin, On the origin and early evolution of terrestrial planet atmospheres and meteoritic volatiles, Icarus 92 (1991) 2–79.

[18] R.O. Pepin, Evolution of Earth's noble gases: consequences of assuming hydrodynamic loss driven by giant impact, Icarus 126 (1997) 148–156.

[19] K.A. Farley, R.J. Poreda, Mantle neon and atmospheric contamination, Earth Planet. Sci. Lett. 114 (1993) 325–339.

[20] P.G. Burnard, F.M. Stuart, G. Turner, Air contamination of basaltic magmas: implications for high $^3He/^4He$ mantle Ar isotopic composition, J. Geophys. Res. 99 (B9) (1994) 17709–17715.

[21] C.J. Ballentine, D.N. Barfod, The origin of air-like noble gases in MORB and OIB, Earth Planet. Sci. Lett. 180 (2000) 39–48.

[22] M.W. Caffee, G.B. Hudson, C. Velsko, G.R. Huss, E.C. Alexander Jr., A.R. Chivas, Primordial noble gases from Earth's mantle: identification of a primitive volatile component, Science 285 (1999) 2115–2118.

[23] D. Porcelli, D. Woolum, P. Cassen, Deep Earth rare gases: initial inventories, capture from the solar nebula, and losses during Moon formation, Earth Planet. Sci. Lett. 193 (2001) 237–251.

[24] F.A. Podosek, D.S. Woolum, P. Cassen, R.H. Nichols, Solar gases in the Earth by solar wind irradiation? 10th Annual Goldschmidt Conf., Oxford, J. Conf. Abstr., vol. 5, 2000, p. 804.

[25] M. Trieloff, J. Kunz, D.A. Clague, D. Harrison, C.J. Allègre, The nature of pristine noble gases in mantle plumes, Science 288 (2000) 1036–1038.

[26] M. Trieloff, J. Kunz, C.J. Allègre, Noble gas systematics of the Réunion mantle plume source and the origin of primordial noble gases in Earth's mantle, Earth Planet. Sci. Lett. 200 (2002) 297–313.

[27] C.L. Harper, S.B. Jacobsen, Noble gases and Earth's accretion, Science 273 (1996) 1814–1818.

[28] D. Porcelli, G.J. Wasserburg, Mass transfer of xenon through a steady-state upper mantle, Geochim. Cosmochim. Acta 59 (1995) 1991–2007.

[29] M. Ozima, G. Igarashi, The primordial noble gases in the Earth: a key constraint on Earth evolution models, Earth Planet. Sci. Lett. 176 (2000) 219–232.

[30] P. Sarda, Surface noble gas recycling to the terrestrial mantle, Earth Planet. Sci. Lett. 228 (2004) 49–63.

[31] K. Marti, K.J. Mathew, Noble gas components in planetary atmospheres and interiors in relation to solar wind and meteorites, Proc. Indian Acad. Sci., Earth Planet. Sci. 107 (1998) 1–7.

[32] D. Phinney, J. Tennyson, U. Frick, Xenon in CO_2 well gas revisited, J. Geophys. Res. 83 (1978) 2313–2319.

[33] T. Staudacher, Upper mantle origin for Harding County well gases, Nature 325 (1987) 605–607.

[34] C.J. Ballentine, B. Marty, B. Sherwood Lollar, M. Cassidy, Neon isotopes constrain convection models and the source of volatiles in the Earth's mantle, Nature 433 (2005) 33–38.

[35] W. Benz, A.G.W. Cameron, Terrestrial effects of the giant impact, in: H.E. Newson, J.H. Jones (Eds.), Origin of the Earth, Oxford University Press, New York, 1991, pp. 61–67.

[36] Th. Staudacher, Ph. Sarda, S.H. Richardson, C.J. Allègre, I. Sagna, L.V. Dmitriev, Noble gases in basalt glasses from a Mid-Atlantic Ridge topographic high at 14°N: geodynamic consequences, Earth Planet. Sci. Lett. 96 (1989) 119–133.
[37] D. York, Least-squares fitting of a straight line, Canadian J. Phys. 44 (1966) 1079–1086.
[38] M. Ozima, F.A. Podosek, G. Igarashi, Terrestrial xenon isotope constraints on the early history of the Earth, Nature 315 (1985) 471–474.
[39] T. Staudacher, C.J. Allègre, Terrestrial xenology, Earth Planet. Sci. Lett. 60 (1982) 389–406.
[40] M. Boyet, R.W. Carlson, ^{142}Nd evidence for early (>4.53 Ga) global differentiation of the silicate Earth, Science 309 (2005) 576–581.
[41] H. Busemann, H. Baur, R. Wieler, Primordial noble gases in "phase Q" in carbonaceous and ordinary chondrites studied by closed-system stepped etching, Meteorit. Planet. Sci. 35 (2000) 949–973.
[42] D. Porcelli, C.J. Ballentine, R. Wieler, An overview of noble gas geochemistry and cosmochemistry, in: D. Porcelli, C.J. Ballentine, R. Wieler (Eds.), Noble Gases in Geochemistry and Cosmochemistry, Rev. Mineral. Geochem., vol. 47, 2002, pp. 1–19.
[43] G.B. Hudson, B.M. Kennedy, F.A. Podosek, C.M. Hohenberg, The early solar system abundance of ^{244}Pu as inferred from the St. Severin chondrite, in: G. Ryder, V.L. Sharpton (Eds.) Proc. Lunar Planet. Sci. Conf. 19th, Cambridge Univ. Press, Cambridge, Lunar and Planetary Institute, Houston, 1989, pp. 547–557.
[44] C.M. Hohenberg, F.A. Podosek, J.R. Reynolds, Xenon–iodine dating: sharp isochronism in chondrites, Science 156 (1967) 233–236.